Adsorption (2013) 19:25–37
DOI 10.1007/s10450-012-9407-1

Experimental and molecular simulation studies of CO_2 adsorption on zeolitic imidazolate frameworks: ZIF-8 and amine-modified ZIF-8

Defei Liu · Yongbiao Wu · Qibin Xia · Zhong Li · Hongxia Xi

Received: 11 April 2012 / Accepted: 20 August 2012 / Published online: 5 September 2012

Abstract ZIF-8 has been rapidly developed as a potential candidate for CO_2 capture due to its low density, high surface area, and robust structure. Considering the electron-donating effect of amino functional groups, amino-modification is expected to be an efficient way to improve CO_2 adsorption of ZIF-8. In this work, grand canonical Monte Carlo (GCMC) simulation was performed to study the CO_2 adsorption isotherm based on ZIF-8, ZIF-8-NH_2, and ZIF-8-$(NH_2)_2$. ZIF-8 was synthesized and CO_2 adsorption isotherms based on ZIF-8 was measured. The experimental surface area, pore volume, and CO_2 adsorption isotherm were used to validate the force field. Adsorptive capacity of ZIF-8-NH_2, and ZIF-8-$(NH_2)_2$ were first estimated. The GCMC simulation results indicated that the order of increasing CO_2 capacity of the ZIF-8 in the lower pressure regime is: ZIF-8 < ZIF-8-NH_2 < ZIF-8-$(NH_2)_2$, and in the high pressure is: ZIF-8 < ZIF-8-$(NH_2)_2$ < ZIF-8-NH_2. New adsorption sites can be generated with the existence of-NH_2 groups. In addition, for non-modified and amino-modified ZIF-8, it was the first time to use density functional theory (DFT) calculations to investigate their CO_2 adsorption sites and CO_2 binding energies. The present work indicates that appropriate amine-functionalized can directly enhanced CO_2 capacity of ZIF-8.

Keywords Molecular simulation · Amino-modification · ZIF-8 · CO_2 adsorption

D. Liu · Y. Wu · Q. Xia · Z. Li · H. Xi (✉)
School of Chemistry and Chemical Engineering, South China University of Technology, Guangzhou, 510641, China
e-mail: cehxxi@scut.edu.cn

1 Introduction

Attempts to solve the greenhouse problem have led to increasing interest in removing CO_2 from the exhaust streams of fossil fuel combustion, which is the first step in carbon sequestration (Sayari et al. 2011; Aaron and Tsouris 2005; Bai and Yeh 1997). However, this step is very difficult to accomplish because of the high temperature and low CO_2 partial pressure flue gas post combustion. Adsorption-based separation technologies exhibit many advantages in dealing with these unfavorable conditions. Therefore, several kinds of materials have been studied for CO_2 adsorption, such as carbon-based materials (Agnihotri et al. 2005; Lu et al. 2008; Su et al. 2009; Choi et al. 2009) and zeolites (Xu et al. 2003; Belmabkhout et al. 2010; Hicks et al. 2008; Krishna and van Baten 2009; Su et al. 2010; Zukal et al. 2010).

Recently, a new class of porous materials known as metal organic frameworks (MOFs) has been synthesized and studied because of its well-defined pores, high surface areas, and desired chemical functionalities (Chen et al. 2010; Tranchemontagne et al. 2008). Additional new MOFs have been synthesized and used in CO_2 adsorption and CO_2 separation process. The so-called zeolitic imidazolate frameworks (ZIFs), most of which have topologies analogous to zeolite structures, are particularly interesting members of the MOF family. They have exceptional chemical and thermal stabilities, and are considered as the promising materials for gas storage and separation (Park et al. 2006; Phan et al. 2009). In addition, several studies have reported the experimental adsorption results of CO_2 on ZIFs. For example, Banerjee et al. (2008) investigated the adsorption of CO_2 on ZIF-69 and found that ZIF-69 had a large adsorption capacity of 82.6 L/L at a low pressure of 1 atm at 298 K. Banerjee et al. (2009) studied the CO_2 adsorption

performance of ZIF-78, and found that ZIF-78 exhibits an extraordinary capacity of 60.2 cm^3/g at 273 K and 1 atm. In fact ZIF-78, one of the best-performing ZIFs, displays a superior ability of storing CO_2 compared to the industrially utilized adsorbent BPL carbon. However, the cost of synthesizing ZIF-78 is too high, especially comparing with its commercial potential. Pérez-Pellitero et al. (2010) reported that the quantity of CO_2 adsorbed on ZIF-8 at lower pressure was lower than that on ZIF-69. But at higher pressure, ZIF-68 achieves a higher CO_2 capacity. These phenomenon could be explained by the fact that the total pore volumes of the ZIF-8 is larger than ZIF-69. It indicated that ZIF-8 is a promising candidate for CO_2 capture.

One feature provoking interest in MOFs is the possibility of modifying desired chemical functionalities to MOF structure. Tuning the affinity of the framework functionalities toward CO_2 is crucial for optimization of the adsorptive properties. Metal-organic frameworks functionalized with amine functional groups have been intensively studied for their enhanced CO_2 adsorption properties (Eddaoudi et al. 2002; Ahnfeldt et al. 2009; Devic et al. 2012; Bauer et al. 2008; Couck et al. 2009; Vaidhyanathan et al. 2009).

In recent years, many researchers, such as Babarao and Jiang (2009), Babarao et al. (2008, 2009), Zhong (Xu et al. 2010; Xue and Zhong 2009; Zheng et al. 2009), Snurr (Bae et al. 2008), Karra and Walton (2010) have investigated the CO_2 adsorption capability of MOF materials using the molecular simulation method. Some attempts have been made to investigate amine modification of IRMOFs (Babarao and Jiang 2008; Mu et al. 2010) and MILs (Arstad et al. 2008; Stavitski et al. 2011; Couck et al. 2012). However, few studies have been performed on molecular simulation regarding amine functionalized ZIFs for CO_2 capture (Morris et al. 2010). Moreover, the mechanism of how the amine-functionalized affects the CO_2 adsorption capability of ZIFs has not been fully understood so far.

In this work, we present an amine-functionalized study for a typical nitrogen containing heterocycles MOF: ZIF-8. The CO_2 adsorption properties of ZIF-8 and amine-functionalized ZIFs [ZIF-8-NH_2 and ZIF-8-$(NH_2)_2$] were investigated by using grand canonical Monte Carlo (GCMC) molecular simulations and density functional theory (DFT) calculations. ZIF-8 was synthesized and characterized by CO_2 adsorption-desorption isotherms, powder XRD, TEM, and Micromeritics ASAP adsorption porosimeter. CO_2 adsorption isotherm was measured to validate the force field. By GCMC calculation, the adsorption site and CO_2 capacity trends of ZIF-8, ZIF-8-NH_2 and ZIF-8-$(NH_2)_2$ were predicted. With the DFT calculation, the electrostatic fields of ZIF-8 and ZIF-8-$(NH_2)_2$ were studied, and the binding energy between CO_2 and these two materials were investigated.

2 Models and simulation method

2.1 ZIF structure

In the present computational study, the structures of ZIF-8 were constructed based on X-ray diffraction (XRD) (Park et al. 2006) patterns using Materials Studio Visualizer (Materials Studio 2009). ZIF-8 has a primitive Zn topology linked by an imidazolate linker. To investigate the amine modification of ZIF-8 simultaneously, two kinds of structures were used in the present study. Different numbers of amino groups were added at two available positions of the imidazolate linker in ZIF-8, near the C=C bond. Then the models were optimized by energy minimization and structure optimization with DFT calculation. In these calculations, the periodic boundary conditions were performed to optimize the structures of their unit cells and the gradient corrected (GGA) correlation functional of PW91 was used with the precise numerical basis set double numerical plus d-functions (DND). The above calculations were carried out with Accelrys $Dmol^3$ code (Materials Studio 2009). All structures are shown in Fig. 1.

2.2 Force field

In the present work, CO_2 was modeled as a rigid linear molecule with three charged Lennard-Jones (LJ) sites located on each atom. A combination of the site–site LJ and Coulomb potentials was used to calculate the CO_2–CO_2 intermolecular interactions. The LJ potential parameters for O and C atoms in CO_2 were taken from the universal force field (UFF) (Rappe et al. 1992). The partial point charges centered at each LJ site (i.e., $q_O = -0.272$ e and $q_C = 0.544$ e) represent the first-order electrostatic and second-order conduction interaction, respectively. This potential model was recently used to successfully simulate the adsorption of CO_2 on ZIF materials (Liu et al. 2009).

For the studied MOFs, an atomistic representation similar to CO_2 was used to model ZIF-8. The same potential model, a combination of the site–site LJ and Coulomb potentials, was used to calculate the interactions between adsorbate molecules and adsorbents. The UFF adopted in this work is able distinguish the type of atoms in the frameworks of the ZIFs materials in detail (Liu et al. 2009). In order to better represent the adsorption isotherms of pure CO_2 on these ZIFs, the calculated part of the atomic partial charges of ZIF-8 by DFT and LJ parameters of the UFF were refined.

The LJ parameters based on this force field were readapted by scaling cohesive energy on the dispersion–repulsion interactions as in equation:

$$\left(\varepsilon_{ij}\sigma_{ij}^6\right)_{\mathrm{New}} = \zeta\left(\varepsilon_{ij}\sigma_{ij}^6\right)_{\mathrm{UFF}}$$

σ_{ij} and ε_{ij} are the crossed LJ parameters obtained between the solid parameters and the CO_2 model of Liu et al. (2009).

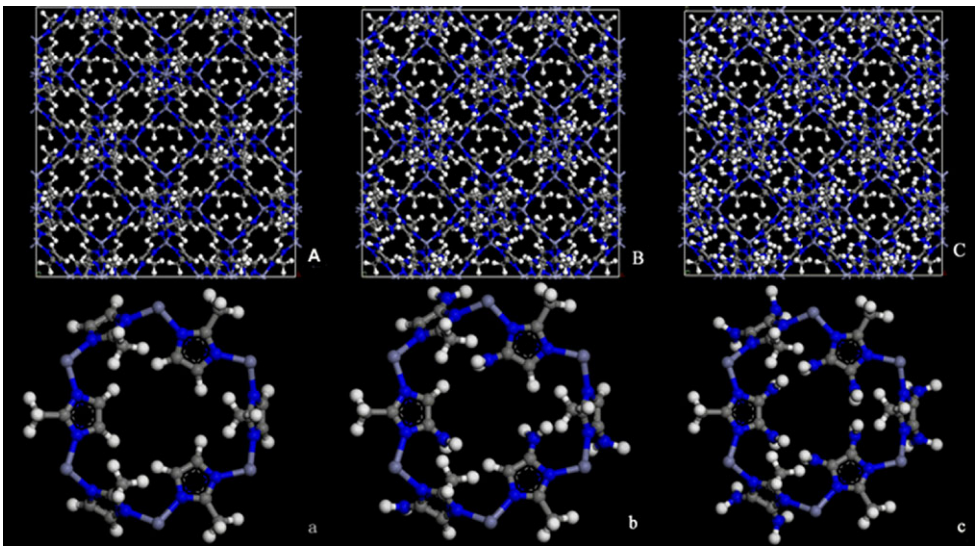

Fig. 1 Crystal structures and cluster of ZIFs used in the simulation: (**A**, **a**) ZIF-8, (**B**, **b**) ZIF-8-NH_2, and (**C**, **c**) ZIF-8-$(NH_2)_2$ (Zn, *purple*; C, *gray*; N, *blue*; H, *white*)

Table 1 LJ Potential parameters for ZIFs in the present work

Atom	σ[a] (Å)	ε/k_B[a] (K)	ε/k_B[b] (K)
CO_2_O	3.12	30.19	
CO_2_C	3.43	52.84	
ZIF_Zn	2.46	62.40	56.10
ZIF_O	3.12	30.19	27.17
ZIF_C	3.43	52.84	47.56
ZIF_N	3.26	34.72	31.25
ZIF_H	2.57	22.14	19.92

[a]taken from UFF

[b]obtained in the present work

Crossed LJ interactions were calculated by applying standard Lorentz-Berthelot combining rules. The parameter ζ was then determined by an iterative procedure to fit the experimental CO_2 isotherm of ZIF-8. A scaling factor of $\zeta \approx 0.899$ was obtained. We then used this factor to adjust the dispersion repulsion parameters for the additional atoms needed to describe host-guest interactions of different gases adsorbed on different ZIFs materials as described in equation (Pérez-Pellitero et al. 2010):

$$(\varepsilon_{ij})_{\text{New}=0.899}(\varepsilon_{ij})_{\text{UFF}}$$

The parameters used are shown in Table 1. The Lorentz-Berthelot combining rules were adopted to calculate the LJ cross-parameters and describe the interaction of the CO_2 molecules with the framework atoms in the ZIF-8 for consistency.

2.3 DFT calculations

The partial charges of the ZIFs were extracted by DFT calculations using the Accelrys Dmol^3 code (Materials Studio 2009). The calculations were performed on the periodic models of ZIF-8 using the PW91 GGA density functional (Perdew and Wang 1992), as well as the double numerical basis set plus polarization (DNP), which is a viable alternative to ab initio methods and can provide reasonable accuracy for computation (Tsuzuki and Luthi 2001). The atomic charges were estimated by the electrostatic potential (ESP) charge method (Mulliken 1955), which has been successfully employed to study the adsorption of CO_2 on ZIFs (Liu et al. 2009; Sirjoosingh et al. 2010). The partial atomic charges of ZIF-8 required in the simulations were showed in Fig. 2.

An important computational study by Torrisi et al. (2010), in which the binding energy (BE) between CO_2 molecule and benzene…X (X = F, Cl, Br, CH_3) molecular complexes were estimated, according to the following schematic equation, in which E_{optim} represents the energy of the system after full geometry relaxation,

$$\text{BE} = E_{\text{optim}}(\text{complex}) - E_{\text{optim}}(\text{ligand}) - E_{\text{optim}}(\text{CO}_2)$$

shows that intermolecular interactions between the CO_2 molecule and a range of functionalized aromatic molecules can be calculated using the DFT theory. Similarly, in this study the BE between CO_2 and the imidazole ring was computed using the same method.

The calculations were performed using PW91/DNP method, as implemented in the Dmol^3 program version (Materials Studio 2009). A real-space orbital global cutoff of 3.7 Å was applied, and the convergence threshold parameters for the optimization were 1×10^{-6} (energy), 2×10^{-4} (gradient), and 5×10^{-3} (displacement). Frequency calculation was performed to determine whether the structure achieved the energy minimization and the distinguishing cases of real energy minima from transition states (TS). A new optimization was performed with more convergence

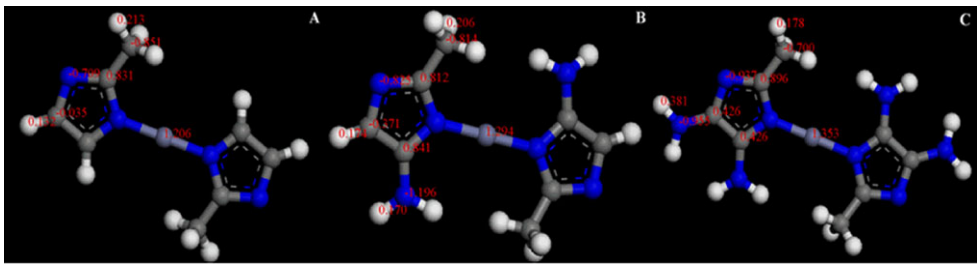

Fig. 2 Partial atomic charges of (**A**) ZIF-8, (**B**) ZIF-8-NH_2, and (**C**) ZIF-8-$(NH_2)_2$ (Zn, *purple*; C, *gray*; N, *blue*; H, *white*)

parameters: 1×10^{-6} (energy), 1×10^{-4} (gradient), and 5×10^{-4} (displacement).

2.4 GCMC simulation

The conventional GCMC simulation technique was employed for calculating gas adsorption isotherms of the CO_2 on ZIF-8, ZIF-8-NH_2, and ZIF-8-$(NH_2)_2$. The simulation box representing ZIFs contained eight ($2 \times 2 \times 2$) unit cells, and periodic boundary conditions were applied in all three dimensions. The simulation with larger boxes showed that no finite-size effects existed. The ZIFs were treated rigidly, and a cut-off radius of 12.8 Å was applied to calculate the LJ interactions. The long-range electrostatic interactions were handled using the Ewald summation technique with a tin-foil boundary condition (Zhang et al. 2007). For each state point, the GCMC simulation consisted of 1×10^6 steps to guarantee equilibration, and the data were collected for another 5×10^6 GCMC steps to obtain the average amount adsorbed.

3 Experimental

3.1 Synthesis of ZIF-8

First, a solid mixture of zinc nitrate hexahydrate $Zn(NO_3)_2 \cdot 6H_2O$ (0.956 g, 3.2 mmol) and 2-methylimidazole (H-MeIM) (0.24 g, 3.4 mmol) was dissolved in 70 mL of DMF solvent. The mixture was quickly transferred to a 100 mL autoclave and sealed. The autoclave was heated at a rate of 5 K/min to 413 K in a programmable oven and held at this temperature for 24 h under autogenous pressure by solvothermal synthesis. Autoclave was then cooled to room temperature at a rate of 0.3 K/min. Chloroform (40 mL) was then added into the autoclave after the removal of the mother liquor from the mixture. The as-synthesized ZIF-8 crystals were isolated by filtration, and the colorless polyhedral crystals were collected from the upper layer, washed thrice with DMF (10 mL), and dried at 383 K overnight (Park et al. 2006). Finally, the as-synthesized ZIF-8 crystals were placed in a quartz tube, which in turn was placed inside a tubular furnace. The samples were maintained under an atmosphere of H_2 (40 mL/min) at 573 K for 120 min, and then cooled to room temperature.

3.2 Characterization

The powder X-ray diffraction (PXRD) patterns of ZIF-8 were taken on a D/max-IIIA (0.5 kW) instrument using Cu-KR radiation of 40 kV and 30 mA at 5° and 25°. The adsorption–desorption isotherms of CO_2 on the ZIF-8 samples were analyzed using a magnetic suspension balance method from Rubotherm, Germany. The surface morphology and particle size of the crystalline ZIF-8 samples were observed by a Philips FEI XL-30 scanning electron microscope at an accelerating voltage of 20 kV. The pore textural properties of the ZIF-8 samples were measured by a Micromeritics ASAP 2020 adsorption porosimeter at a liquid nitrogen temperature of 77 K. The Brunauer-Emmet-Teller (BET) area, Langmuir surface area, and pore volume were obtained.

4 Results and discussion

4.1 Structure stability and force field validation

From the structure optimization results, the unit cell lengths of ZIF-8-NH_2 and ZIF-8-$(NH_2)_2$ are 16.81 and 16.72, which are very close to that of ZIF-8 (16.99 Å). Figure 1 shows the optimized unit cell crystal structures of ZIF-8-NH_2 and ZIF-8-$(NH_2)_2$. As can be seen from Fig. 1, the optimized crystal structures do not collapse and keep the similar SOD topologies as that of ZIF-8. These results indicate that the structures of amine-modified ZIF-8 are stable and can be further used for the following investigations in this work.

GCMC simulations were performed to calculate the adsorption isotherm of CO_2 on ZIF-8 in the pressure range from 0 to 30 atm at 298 K. The calculated isotherms and the experimental values are shown in Fig. 3. The simulated results calculated with the UFF LJ parameters are much higher than the experimental results. In regards to the accuracy of the measurement, the results calculated with new parameters are in better agreement with the experimental results for CO_2 isotherm. The simulated surface area and pore volume (showed in Table 3) calculated with simple GCMC and the new LJ parameters also present acceptable accuracy. These results demonstrate that the model and the new force field parameters used in the present work accurately describe the CO_2 adsorption behavior on ZIF-8.

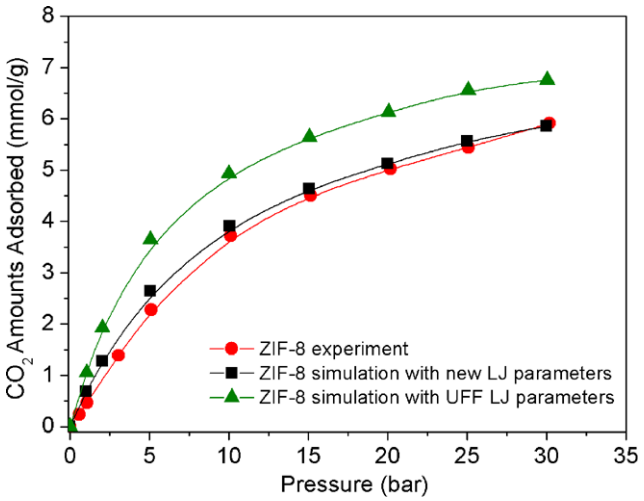

Fig. 3 Comparison of the simulated and experimental CO_2 adsorption isotherms on ZIF-8 at 298 K

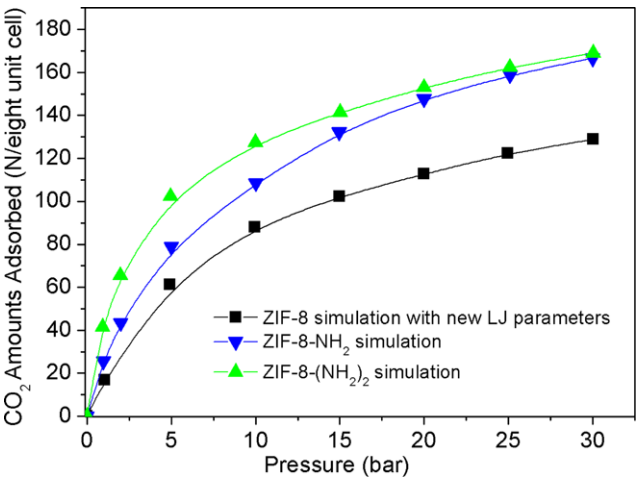

Fig. 4 CO_2 adsorption isotherm on ZIF-8, ZIF-8-$(NH_2)_2$, and ZIF-8-NH_2 at 298 K, as investigated by GCMC simulation (expressed in N/eight unit cell)

4.2 CO_2 adsorption isotherm simulation of ZIF-8 and amine-modified ZIF-8

To investigate the adsorption enhancement of amine-modified ZIFs produced by the grafting of amino functional groups, additional GCMC simulations were performed on the ZIF-8-$(NH_2)_2$ and CO_2 molecules. The calculated isotherms, expressed in $N_{molecules}$/eight unit cell, are shown in Fig. 4 at low and high pressure. The data indicates that the capacity for CO_2 adsorption on ZIF-8-$(NH_2)_2$ and ZIF-8-NH_2 is much better than that on ZIF-8. This phenomenon is attributed to two reasons. First, the basic amino groups have a high affinity toward acidic CO_2 mainly through the interaction with the lone electron pair on nitrogen. Second, quadrupole-π electron interaction between CO_2 molecule and imidazole ring is strengthened by the electron-donating group (amino functional groups). In essence, the more the electron-donating groups (amino functional groups) are added, the stronger the quadrupole-π electron interaction is. Thus, at lower pressure, the capacity of CO_2 adsorption on ZIF-8-$(NH_2)_2$ is better than on ZIF-8-NH_2. Moreover, at higher pressure, the capacity for CO_2 adsorption of ZIF-8-$(NH_2)_2$ is nearly the same as that on ZIF-8-NH_2. That is because at higher pressure, the adsorption sites near the methyl contribute to the CO_2 adsorption. However these adsorption sites are weakened by the addition of amino functional groups.

The simulated CO_2 adsorption isotherm on ZIF-8 and the simulated CO_2 adsorption isotherm on ZIF-8-$(NH_2)_2$ and ZIF-8-NH_2 at 298 K are shown in Fig. 5. All adsorption quantities in adsorption isotherms are expressed in mmol/g. Results of the adsorption isotherm obtained from the simulation shows that, at lower pressure (below 12 bar), the CO_2 adsorption quantity on ZIF-8-$(NH_2)_2$ is higher than

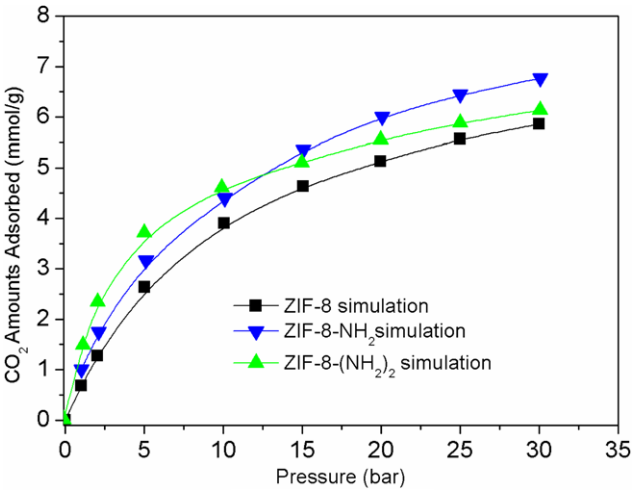

Fig. 5 The simulated CO_2 adsorption isotherm on ZIFs at 298 K

that on ZIF8-NH_2. The order of CO_2 capacity of ZIF-8 is: ZIF-8 < ZIF-8-NH_2 < ZIF-8-$(NH_2)_2$. However at higher pressure (above 12 bar), the CO_2 adsorption quantity on ZIF-8-$(NH_2)_2$ is much lower than ZIF-8-NH_2, which differs from the result shown in Fig. 4. The order of CO_2 capacity of the ZIF-8's is, ZIF-8 < ZIF-8-$(NH_2)_2$ < ZIF-8-NH_2. This is likely because the numbers of adsorption sites on the ZIFs increased with the addition of amino functional groups, which also increased the framework mass (11.7 %). At lower pressure, the more amino functional groups added into ZIF-8 structure, the larger the adsorption quantity. However, the opposite occurs at higher pressure, indicating that the adsorption quantity can be improved only when appropriate numbers of amino functional groups are added.

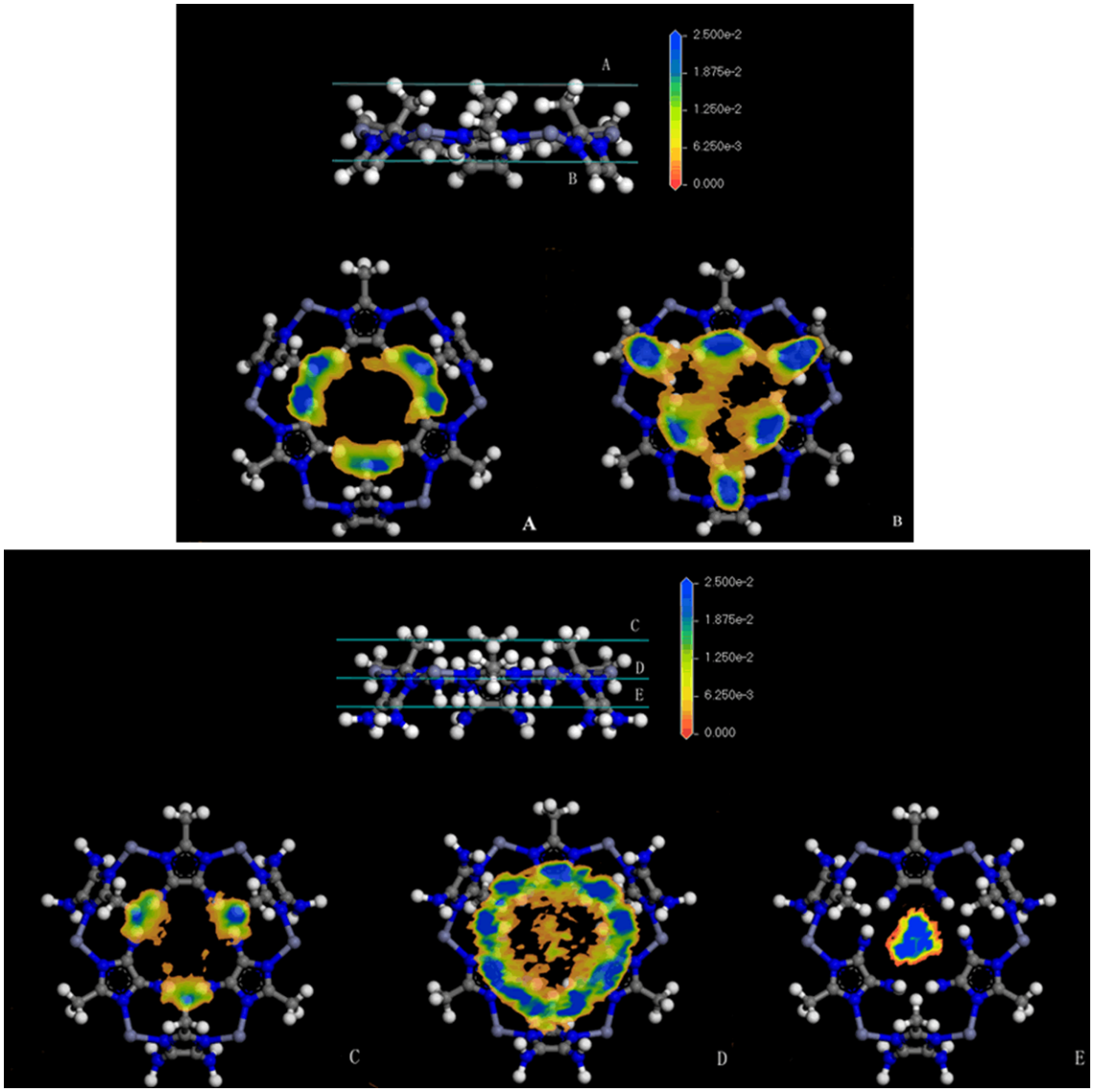

Fig. 6 Sliced images [(111) view] of the different positions of the ZIF-8 and ZIF-8-$(NH_2)_2$ structure. (**A**) above the three methyl rings; (**B**) near the six imidazole rings of the ZIF-8 structure; (**C**) the three methyl rings of ZIF-8-$(NH_2)_2$; (**D**) near the imidazole ring of ZIF-8-$(NH_2)_2$; and (**E**) in the middle of the six amidogen rings of ZIF-8-$(NH_2)_2$

4.3 Adsorption sites in ZIFs

Knowledge of adsorption sites is important in understanding the adsorption mechanism. Therefore, the center of mass (COM) probability distributions of adsorbate CO_2 on ZIF-8 was calculated based on all the configurations recorded during the GCMC simulations. The COM map of ZIF-8 and ZIF-8-$(NH_2)_2$ near the Zn-hexagon opening was also sliced to form the unit cell of ZIF-8 and ZIF-8-$(NH_2)_2$ with certain rules (Zhou et al. 2009). The sliced images [(111) view] of different positions are plotted in Fig. 6. Several color fields (blue–green–yellow) are used to indicate the adsorption sites of CO_2 on ZIF-8 and ZIF-8-$(NH_2)_2$. The blue represents the highest quantity of CO_2 adsorbed and the yellow represents the least adsorbed. The most important adsorption site in ZIF-8 is above the three methyl rings (Plane A) and near the six imidazole rings (Plane B). Besides the three methyl rings (Plane C) and near the imidazole ring (Plane D) in ZIF-8-$(NH_2)_2$, another adsorption site can be found in the middle of six amidogen rings (Plane E); this new adsorption site likely appeared when the electron-donating group (amino functional groups) was added into the ZIF-8.

4.4 Relationship between the electrostatic fields in ZIFs and the CO_2 adsorption capacity

To investigate the effects of the electron-donating groups on the adsorption site, the electrostatic potentials (Babarao

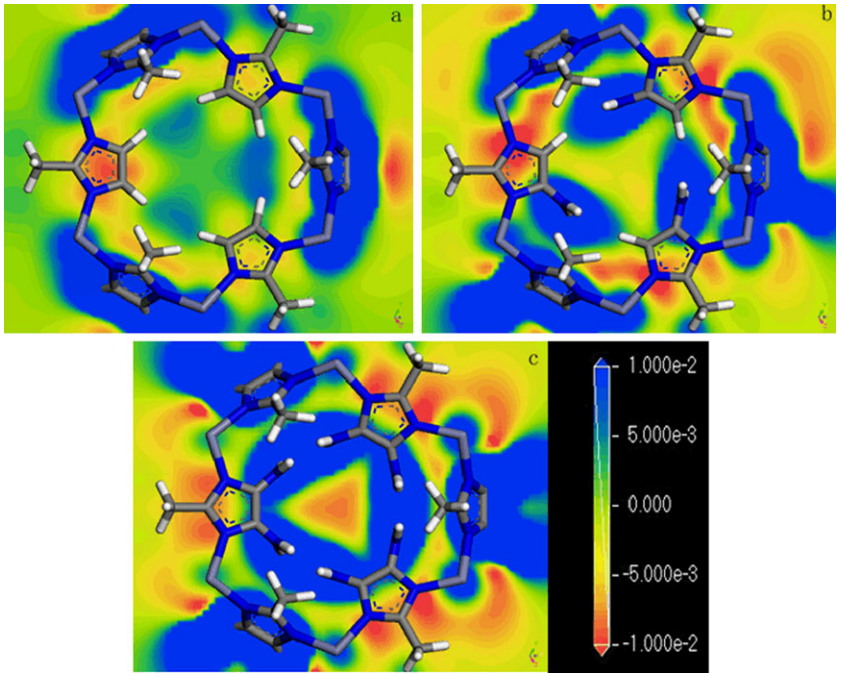

Fig. 7 Contour maps of ESP for (**a**) ZIF-8, (**b**) ZIF-8-NH_2, and (**c**) ZIF-8-$(NH_2)_2$

and Jiang 2008; Mu et al. 2010) for ZIF8, ZIF8-NH_2, and ZIF8-$(NH_2)_2$ were studied to determine the enhanced electrostatic interactions of CO_2 molecules within the frameworks. The contour maps of the ESPs were calculated using Dmol^3, as implemented in the Materials Studio package (Materials Studio 2009), to obtain the gradient of potential changes and reflect the strength of the electrostatic field in the pore of the ZIFs. The values should influence the polarization of the CO_2 molecules within the ZIFs cavities, as shown in Fig. 7. An ESP with a larger gradient and higher absolute values is near the organic linker and imidazole ring, reflecting a stronger electrostatic field in the pores of ZIF8-$(NH_2)_2$ than that in ZIF8-NH_2 and ZIF8. The reason is that amino functional groups not only provide the lone pair electrons, but also significantly enhance the π electrons interaction on the imidazole ring. According to the adsorption isotherms and adsorption sites obtained from the GCMC simulation, higher CO_2 adsorption and new adsorption sites on ZIF8-$(NH_2)_2$ and ZIF8-NH_2 were caused by the electrostatic field enhancement from the amino functional groups. Overall, these observations are in good agreement with the results shown in Fig. 5.

4.5 DFT calculation of BE

Figure 8 shows three different stable configurations for the complex $C_4H_6N_2\cdots CO_2$. The most stable conformation has the CO_2 on the imidazole ring top position (Fig. 8, dimer A, BE = -7.741 kJ mol^{-1}), with C(CO_2) at a distance of 3.556 and 3.958 Å from two imidazole ring N atoms and 4.494 Å from the methyl C atom. The stability of the conformation is caused by the quadrupole-π electron interaction between the π electrons on the imidazole ring and the electron-deficient carbon of the CO_2 molecule, as well as by the weak interaction between the methyl and CO_2 molecule.

A second, less stable configuration has the CO_2 positioned beside the methyl group with the shortest distance O(CO_2)$\cdots$H(methyl) of 3.239 Å (Fig. 8, dimer B, BE = -3.43 kJ mol^{-1}) because there is a hydrogen bond-like interaction between O(CO_2) and H(methyl).

The least stable configuration (Fig. 8, dimer C, BE = -4.85 kJ mol^{-1}) has the CO_2 located at the side of the molecule, which is roughly perpendicular to the imidazole ring and on the opposite side to the methyl group. There is O(CO_2)-H(imidazole ring) at distances of 3.252 and 3.236 Å, likely stabilized by a very weak electrostatic interaction between one of the oxygens of CO_2 (roughly in the plane of the ring) and the positive electrostatic potential of the imidazole hydrogen.

Three stable configurations of the $C_4H_8N_4\cdots CO_2$ complex were identified. The most stable one (Fig. 9, dimer A, BE = -9.76 kJ mol^{-1}) shows that CO_2 is positioned between two amino functional groups, with a C(CO_2)$\cdots$N(amino functional groups) interactions at 3.726 and 3.039 Å. This configuration is stabilized by the electrostatic interaction between the lone pair nitrogen electrons of two amino groups and the electron-deficient carbon of the CO_2 molecule.

Another stable configuration with BE of -7.90 kJ mol^{-1} (Fig. 9, dimer B) corresponds to CO_2 on top of the imidazole ring position with a C(CO)$_2\cdots$N(imidazole ring) dis-

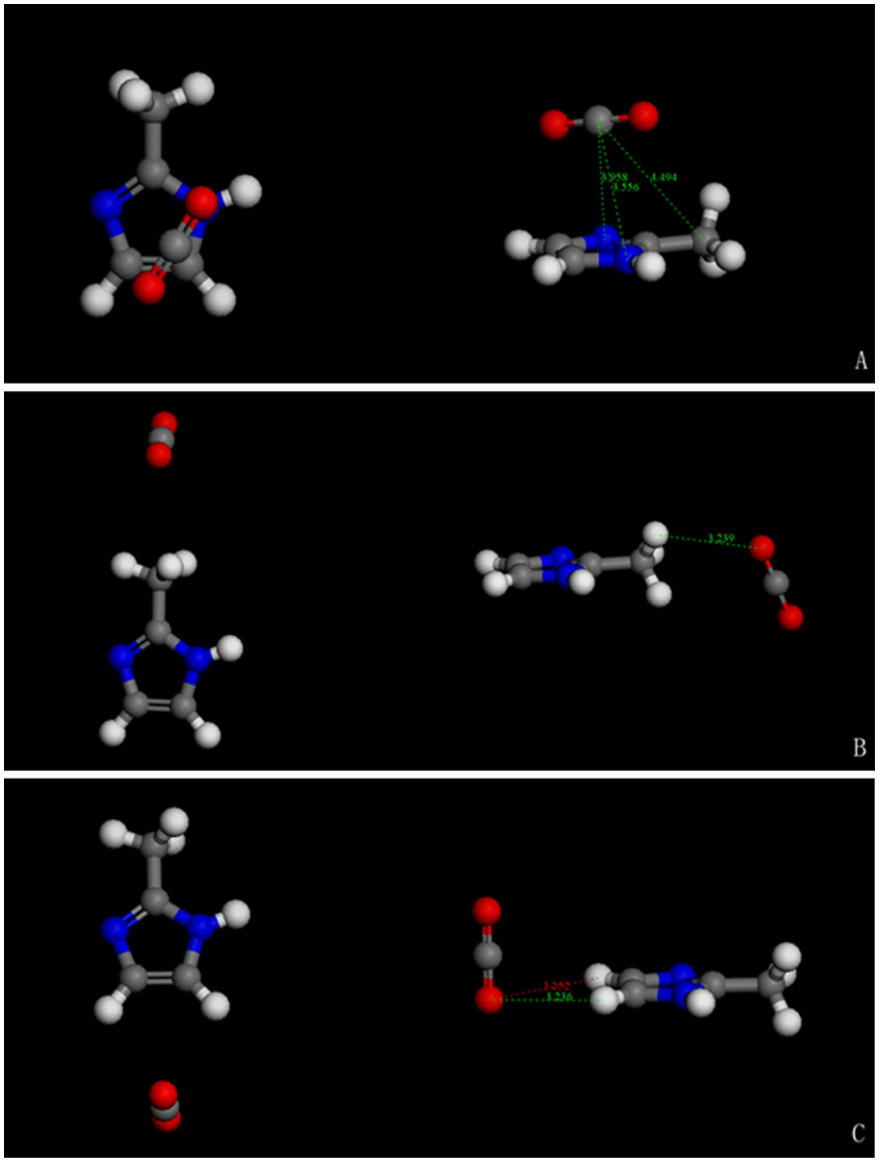

Fig. 8 DFT-optimized stable configurations of the complex $C_4H_6N_2 \cdots CO_2$ in ZIF-8

tance of 4.147 and 3.931 Å, and with a $C(CO)_2 \cdots N$(amino functional groups) distance of 3.481 and 3.891 Å. This configuration is considered a quadrupole-π electron interaction between the CO_2 molecule and imidazole ring.

The third stable configuration with BE of -2.16 kJ mol^{-1} (Fig. 9, dimer C) corresponds to CO_2 positioned beside the methyl group because of the interaction between $O(CO_2)$ and methyl H; the shortest distance of $O(CO_2) \cdots C$(methyl) is 3.133 Å.

The present work studies the BEs of above stable configurations. When the amino functional groups were added into the imidazole ring, the BE between CO_2 and methyl was reduced, indicating that the CO_2 adsorption capacity near the methyl was also reduced. The configuration of CO_2, when positioned between two amino functional groups, has the largest BE, indicating that the CO_2 adsorption ability between two amino functional groups was much stronger than the configuration with no amino functional groups. In addition, the quadrupole-π electron interaction between CO_2 and imidazole ring can be improved by an electron-donating group (e.g. amino functional groups).

Recently, several research groups reported that amine groups anchored on linkers of MIL structures have no direct effect on CO_2 adsorption (Arstad et al. 2008; Serra-Crespo et al. 2011; Stavitski et al. 2011). The most typical result is reported by Stavitski et al. (2011), they demonstrated that the adsorption of CO_2 moleculars on MIL-53 is directed by the formation of hydrogen bonding between CO_2 and bridging –OH groups located at the $[AlO_6]$ unit. However, it was easier to form the hydrogen bond between CO_2 and bridging –OH groups due to the interaction between the adjacent $[AlO_6]$ unit and $–NH_2$ group. They also found that hydrogen

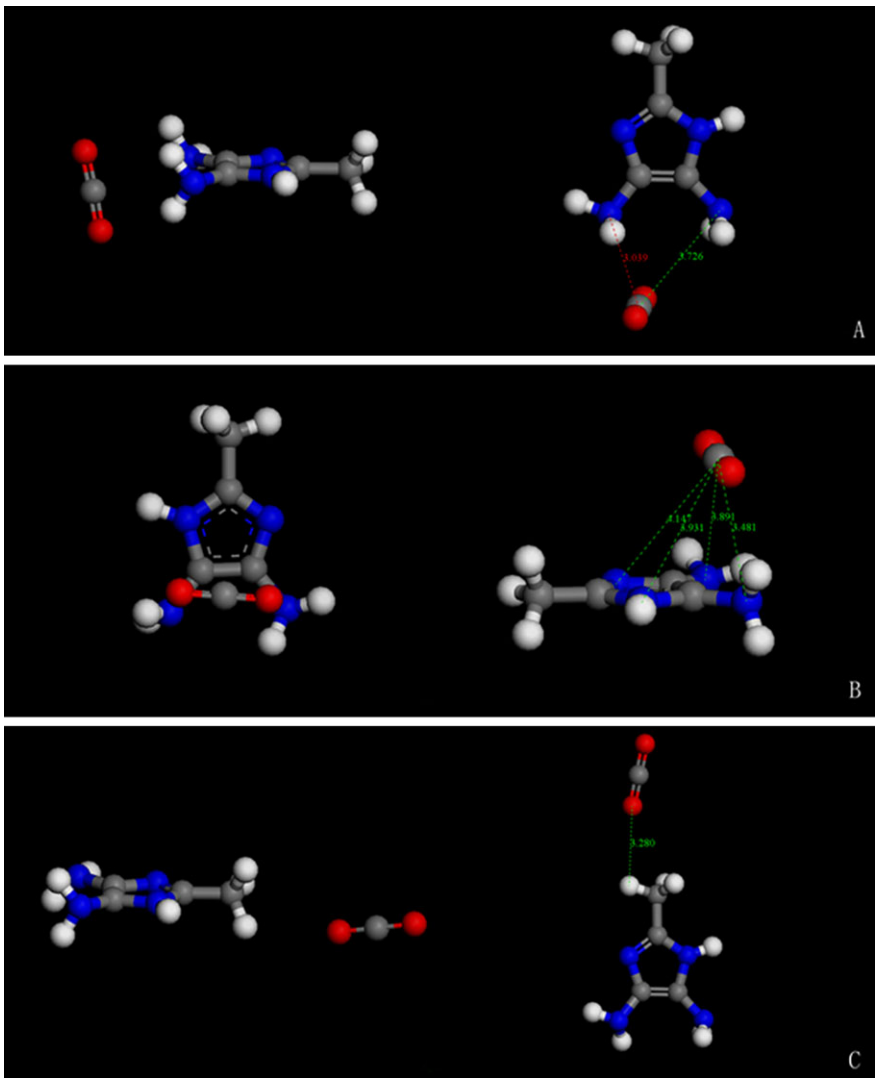

Fig. 9 DFT-optimized stable configurations of the complex $C_4H_8N_4 \cdots CO_2$ in ZIF-8-$(NH_2)_2$

bond between $-NH_2$ groups and $[AlO_6]$ made the flexible NH_2-MIL-53(Al) much more easy to form a narrow pore structure (np NH_2-MIL-53(Al)). Both of the above interactions reduce the electron-donating effect of $-NH_2$ group. So no direct strong interaction between CO_2 and the amino group are observed. Compared with the present results, the major adsorption site of CO_2 on ZIF-8 is near imidazole rings instead of metal oxides cluster (ZIFs have no metal oxides cluster, such as $[AlO_6]$ or $[CrO_6]$). The main interaction is between organic linker and CO_2. For ZIF-8-NH_2 and ZIF-8-$(NH_2)_2$, there is no hydrogen bond between $-NH_2$ groups and metal oxides cluster. Therefore, $-NH_2$ groups on imidazolate ring can directly affect the CO_2 molecules. Moreover, the $-NH_2$ groups also contribute to quadrupole-π electron interaction of imidazolate rings and the interaction with CO_2. Hence, interaction between CO_2 and $-NH_2$ groups are still strong.

4.6 Experimental section of ZIF-8

The single-crystal PXRD images of the synthesized ZIF-8 sample are shown in Fig. 10. The well-formed peaks imply the high crystallinity of the ZIF-8 samples. Table 2 shows that the main peak in PXRD and the main peaks of the ZIF-8 sample are in conformity with the XRD patterns for the sample synthesized by Yaghi et al. (Park et al. 2006).

The SEM picture in Fig. 11 shows that the particles were micron scale with sharp hexagonal facets. The mean particle size is $\sim$2 μm. The N_2 adsorption measurement in Fig. 12 shows the type I isotherm. The increase in the volume adsorbed at low relative pressures is due to the presence of micropores; while a second uptake at high relative pressure indicates existence of textural meso/macroporosity formed by packing of nanoparticles. The microporous pore volume is about 0.47 $cm^3\,g^{-1}$, and the BET (showed in Table 3) and Langmuir surface areas are 1070 and 1243 $m^2\,g^{-1}$, respec-

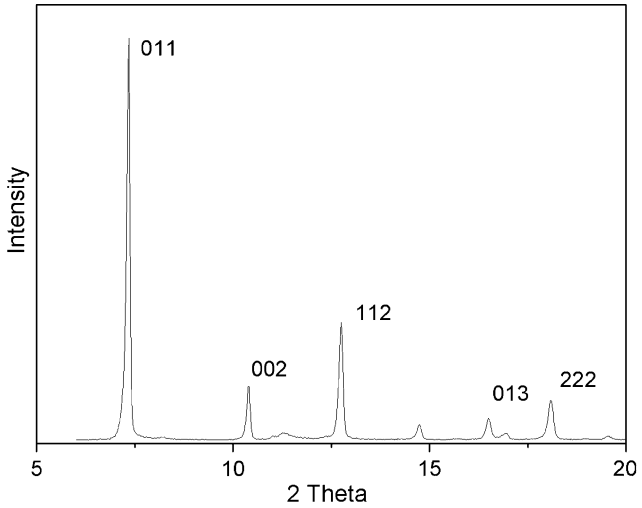

Fig. 10 Single-crystal PXRD of ZIF-8 synthesized in the present work

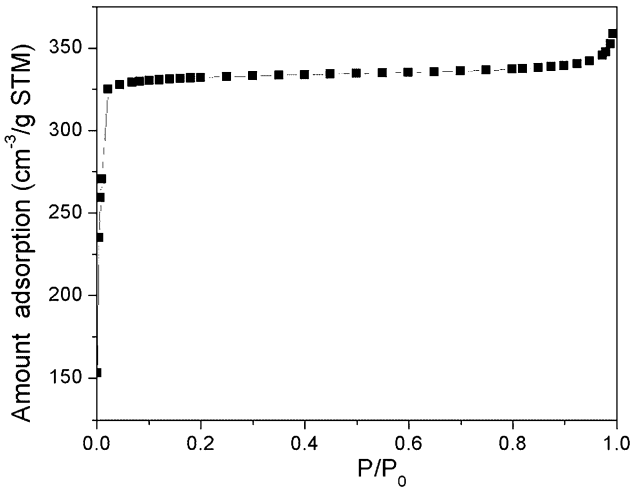

Fig. 12 Nitrogen sorption isotherms of as-synthesized ZIF-8 crystals at 77 K

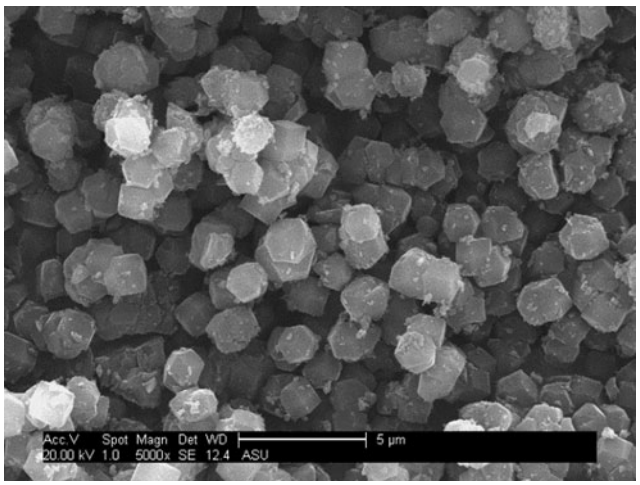

Fig. 11 SEM picture of ZIF-8 crystals

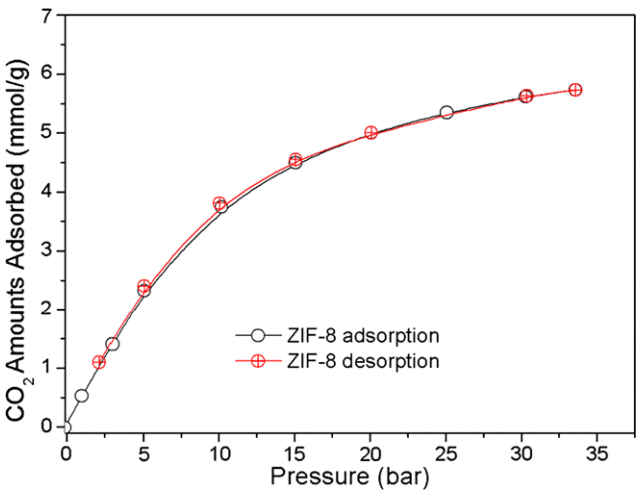

Fig. 13 CO_2 adsorption–desorption isotherm on ZIF-8 and amine–modified ZIF-8

Table 2 Main peaks in powder single-crystal X-ray diffraction of ZIF-8 samples

ZIF8 sample synthesized in the present work		Sample synthesized by Yaghi et al.	
2-Theta	hkl	2-Theta	hkl
7.29	011	7.35	011
10.32	002	10.40	002
12.65	112	12.75	112
16.50	013	16.48	013
18.01	222	18.07	222

Table 3 The pore textural properties of the studied ZIFs

	Surface area S_a[a] (m^2/g) exptl/calcd	Pore volume V_p[b] (cm^3/g) exptl/calcd
ZIF-8	1070/1132.11	0.47/0.42
ZIF-8-NH_2	NA/1014.32	NA/0.37
ZIF-8-$(NH_2)_2$	NA/908.32	NA/0.35

[a]The simulated surface area was calculated by simple Monte Carlo simulation program with the new force field list above (Duren and Snurr 2004)

[b] V_p is the free volume within adsorbent for adsorption estimated from N_2 GCMC simulations (Myers 2002)

tively. The BET surface area is near the values that were reported for other ZIF-8 samples (Park et al. 2006).

Figure 13 shows the CO_2 adsorption-desorption isotherm on ZIF-8. The desorption isotherm of ZIF-8 material is nearly the same as the adsorption isotherm. The CO_2

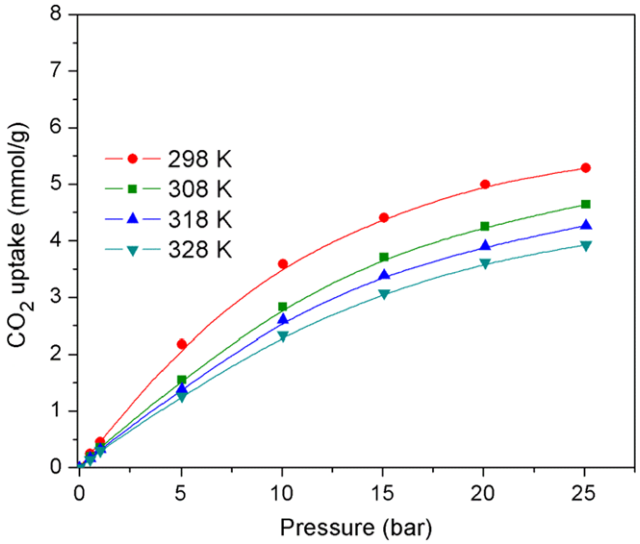

Fig. 14 Isotherms of CO_2 on ZIF-8 with different temperatures

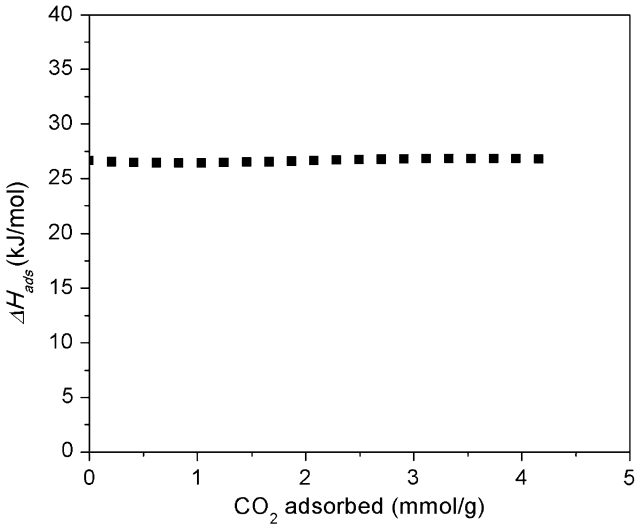

Fig. 15 Dependence of enthalpy of adsorption on the amounts adsorbed of CO_2 over ZIF-8

adsorption–desorption isotherm indicates that ZIF-8 material show micropore adsorption behavior.

To further understand the adsorption properties, the enthalpy of adsorption (ΔH_{ads}) of CO_2 was determined by measuring a series of isotherms at 298 K, 308 K, 318 K, 328 K and fitting the data to the virial model. The enthalpy of adsorption (ΔH_{ads}) for ZIF-8 is 26.7 kJ/mol (see Figs. 14 and 15).

5 Conclusion

GCMC simulations were carried out to investigate the CO_2 adsorption isotherms and adsorption sites on ZIF-8 and amine-modified ZIF-8. Results of the CO_2 adsorption isotherm simulation of ZIF-8 are consistent with the experimental results obtained. It shows that the parameters applied in the present work are in agreement with the experimental data. The GCMC simulation results also show that the CO_2 adsorption ability of ZIF-8 can be enhanced by the addition of amino functional groups. The results of CO_2 adsorption sites on ZIF-8 and ZIF-8-$(NH_2)_2$ indicated that the adsorption sites on ZIF-8 are near the imidazole rings and above the three methyl rings. On ZIF-8-$(NH_2)_2$, there is a new adsorption site in the middle of six amidogen rings beside the two adsorption sites above, as supported by the electrostatic field and BE investigations. We find that the quadrupole-π electron interaction between the CO_2 molecule and the imidazole ring in the ZIF-8 structure is strengthened by the electron donating amino groups. We also propose that $-NH_2$ groups on imidazolate ring can directly affect the CO_2 molecules. Hence, CO_2 adsorption capacity on ZIF-8 can be increased by the addition of $-NH_2$ groups.

Acknowledgements Financial support from the National Natural Science Foundation of China (Nos. 20936001 and 21176084), and Guangdong Natural Science Foundation (S2011030001366) are gratefully acknowledged.

References

Aaron, D., Tsouris, C.: Separation of CO_2 from flue gas: a review. Sep. Sci. Technol. **40**(1–3), 321–348 (2005)

Agnihotri, S., Rood, M.J., Rostam-Abadi, M.: Adsorption equilibrium of organic vapors on single-walled carbon nanotubes. Carbon **43**(11), 2379–2388 (2005). doi:10.1016/j.carbon.2005.04.020

Ahnfeldt, T., Gunzelmann, D., Loiseau, T., Hirsemann, D., Senker, J., Ferey, G., Stock, N.: Synthesis and modification of a functionalized 3D open-framework structure with MIL-53 topology. Inorg. Chem. **48**(7), 3057–3062 (2009)

Arstad, B., Fjellvåg, H., Kongshaug, K., Swang, O., Blom, R.: Amine functionalised metal organic frameworks (MOFs) as adsorbents for carbon dioxide. Adsorption **14**(6), 755–762 (2008). doi:10.1007/s10450-008-9137-6

Babarao, R., Jiang, J.: Molecular screening of metal–organic frameworks for CO_2 storage. Langmuir **24**(12), 6270–6278 (2008). doi:10.1021/la800369s

Babarao, R., Jiang, J.: Unprecedentedly high selective adsorption of gas mixtures in rho zeolite-like metal–organic framework: a molecular simulation study. J. Am. Chem. Soc. **131**(32), 11417–11425 (2009). doi:10.1021/ja901061j

Babarao, R., Jiang, J., Sandler, S.I.: Molecular simulations for adsorptive separation of CO_2/CH_4 mixture in metal-exposed, catenated, and charged metal–organic frameworks. Langmuir **25**(9), 5239–5247 (2008). doi:10.1021/la803074g

Babarao, R., Tong, Y.H., Jiang, J.W.: Molecular insight into adsorption and diffusion of alkane isomer mixtures in metal-organic frameworks. J. Phys. Chem. B **113**(27), 9129–9136 (2009). doi:10.1021/jp902253p

Bae, Y.-S., Mulfort, K.L., Frost, H., Ryan, P., Punnathanam, S., Broadbelt, L.J., Hupp, J.T., Snurr, R.Q.: Separation of CO_2 from CH_4 using mixed-ligand metal−organic frameworks. Langmuir **24**(16), 8592–8598 (2008). doi:10.1021/la800555x

Bai, H., Yeh, A.C.: Removal of CO_2 greenhouse gas by ammonia scrubbing. Ind. Eng. Chem. Res. **36**(6), 2490–2493 (1997). doi:10.1021/ie960748j

Banerjee, R., Phan, A., Wang, B., Knobler, C., Furukawa, H., O'Keeffe, M., Yaghi, O.M.: High-throughput synthesis of zeolitic imidazolate frameworks and application to CO_2 capture. Science **319**(5865), 939–943 (2008). doi:10.1126/science.1152516

Banerjee, R., Furukawa, H., Britt, D., Knobler, C., O'Keeffe, M., Yaghi, O.M.: Control of pore size and functionality in isoreticular zeolitic imidazolate frameworks and their carbon dioxide selective capture properties. J. Am. Chem. Soc. **131**(11), 3875–3877 (2009). doi:10.1021/ja809459e

Bauer, S., Serre, C., Devic, T., Horcajada, P., Marrot, J., Ferey, G., Stock, N.: High-throughput assisted rationalization of the formation of metal organic frameworks in the iron(III) aminoterephthalate solvothermal system. Inorg. Chem. **47**(17) (2008). doi:10.1021/ic800538r

Belmabkhout, Y., Serna-Guerrero, R., Sayari, A.: Adsorption of CO_2-containing gas mixtures over amine-bearing pore-expanded MCM-41 silica: application for gas purification. Ind. Eng. Chem. Res. **49**(1), 359–365 (2010)

Chen, B., Wang, X., Zhang, Q., Xi, X., Cai, J., Qi, H., Shi, S., Wang, J., Yuan, D., Fang, M.: Synthesis and characterization of the interpenetrated MOF-5. J. Mater. Chem. **20**(18) (2010). doi:10.1039/B922528E

Choi, S., Drese, J.H., Jones, C.W.: Adsorbent materials for carbon dioxide capture from large anthropogenic point sources. ChemSusChem **2**(9), 796–854 (2009)

Couck, S., Denayer, J.F.M., Baron, G.V., Remy, T., Gascon, J., Kapteijn, F.: An amine-functionalized MIL-53 metal-organic framework with large separation power for CO_2 and CH_4. J. Am. Chem. Soc. **131**(18), 6326–6327 (2009)

Couck, S., Gobechiya, E., Kirschhock, C.E.A., Serra-Crespo, P., Juan-Alcaniz, J., Joaristi, A.M., Stavitski, E., Gascon, J., Kapteijn, F., Baron, G.V., Denayer, J.F.M.: Adsorption and separation of light gases on an amino-functionalized metal-organic framework: an adsorption and in situ XRD study. ChemSusChem **5**(4), 740–750 (2012)

Devic, T., Vimont, A., Greneche, J., Moreau, F., Magnier, E., Filinchuk, Y., Marrot, J., Lavalley, J., Daturi, M., Ferey, G.: Functionalization in flexible porous solids: effects on the pore opening and the host-guest interactions. J. Am. Chem. Soc. **132**(3), 1127–1136 (2012)

Duren, T., Snurr, R.Q.: Assessment of isoreticular metal-organic frameworks for adsorption separations: a molecular simulation study of methane/n-butane mixtures. J. Phys. Chem. B. **108**(40) (2004)

Eddaoudi, M., Kim, J., Rosi, N., Vodak, D., Wachter, J., O'Keeffe, M., Yaghi, O.M.: Systematic design of pore size and functionality in isoreticular MOFs and their application in methane storage. Science **295**(18), 469–471 (2002)

Hicks, J.C., Drese, J.H., Fauth, D.J., Gray, M.L., Qi, G.G., Jones, C.W.: Designing adsorbents for CO_2 capture from flue gas-hyperbranched aminosilicas capable of capturing CO_2 reversibly. J. Am. Chem. Soc. **130**(10), 2902–2903 (2008)

Karra, J.R., Walton, K.S.: Molecular simulations and experimental studies of CO_2, CO, and N_2 adsorption in metal organic frameworks. J. Phys. Chem. C **114**(37), 15735–15740 (2010)

Krishna, R., van Baten, J.M.: Comment on comparative molecular simulation study of CO_2/N_2 and CH_4/N_2 separation in zeolites and metal–organic frameworks. Langmuir **26**(4), 2975–2978 (2009). doi:10.1021/la9041875

Liu, D., Zheng, C., Yang, Q., Zhong, C.: Understanding the adsorption and diffusion of carbon dioxide in zeolitic imidazolate frameworks: a molecular simulation study. J. Phys. Chem. C **113**(12), 5004–5009 (2009). doi:10.1021/jp809373r

Lu, C., Bai, H., Wu, B., Su, F., Hwang, J.F.: Comparative study of CO_2 capture by carbon nanotubes, activated carbons, and zeolites. Energy Fuels **22**(5), 3050–3056 (2008). doi:10.1021/ef8000086

Materials Studio: Materials Studio 4.4. v. Accelrys, Inc., San Diego (2009)

Morris, W., Leung, B., Furukawa, H., Yaghi, O.K., Hayashi, H., Houndonougbo, Y., Asta, M., Laird, B.B., Yaghi, O.M.: A combined experimental-computational investigation of carbon dioxide capture in a series of isoreticular zeolitic imidazolate frameworks. J. Am. Chem. Soc. **132**(32) (2010)

Mu, W., Liu, D., Yang, Q., Zhong, C.: Computational study of the effect of organic linkers on natural gas upgrading in metal–organic frameworks. Microporous Mesoporous Mater. **130**(1–3), 76–82 (2010). doi:10.1016/j.micromeso.2009.10.015

Mulliken, R.S.: Electronic population analysis on LCAO-MO molecular wave functions. J. Chem. Phys. **23**, 1833–1840 (1955)

Myers, A.L.: Adsorption in porous materials at high pressure: theory and experiment. Langmuir **18**(26) (2002)

Pérez-Pellitero, J., Amrouche, H., Siperstein, F.R., Pirngruber, G., Nieto-Draghi, C., Chaplais, G., Simon-Masseron, A., Bazer-Bachi, D., Peralta, D., Bats, N.: Adsorption of CO_2, CH_4, and N_2 on zeolitic imidazolate frameworks: experiments and simulations. Chem., Eur. J. **16**(5), 1560–1571 (2010). doi:10.1002/chem.200902144

Park, K.S., Ni, Z., Côté, A.P., Choi, J.Y., Huang, R., Uribe-Romo, F.J., Chae, H.K., O'Keeffe, M., Yaghi, O.M.: Exceptional chemical and thermal stability of zeolitic imidazolate frameworks. Proc. Natl. Acad. Sci. USA **103**(27), 10186–10191 (2006). doi:10.1073/pnas.0602439103

Perdew, J.P., Wang, Y.: Accurate and simple analytic representation of the electron-gas correlation energy. Phys. Rev. B **45**(23), 13244–13249 (1992)

Phan, A., Doonan, C.J., Uribe-Romo, F.J., Knobler, C.B., O'Keeffe, M., Yaghi, O.M.: Synthesis, structure, and carbon dioxide capture properties of zeolitic imidazolate frameworks. Acc. Chem. Res. **43**(1), 58–67 (2009). doi:10.1021/ar900116g

Rappe, A.K., Casewit, C.J., Colwell, K.S., Goddard, W.A., Skiff, W.M.: UFF, a full periodic table force field for molecular mechanics and molecular dynamics simulations. J. Am. Chem. Soc. **114**(25), 10024–10035 (1992). doi:10.1021/ja00051a040

Sayari, A., Belmabkhout, Y., Serna-Guerrero, R.: Flue gas treatment via CO_2 adsorption. Chem. Eng. J. **171**(3), 760–774 (2011)

Serra-Crespo, P., Ramos-Fernandez, E.V., Gascon, J., Kapteijn, F.: Synthesis and characterization of an amino functionalized MIL-101(Al): separation and catalytic properties. Chem. Mater. **23**, 2565–2572 (2011)

Sirjoosingh, A., Alavi, S., Woo, T.K.: Grand-canonical Monte Carlo and molecular-dynamics simulations of carbon-dioxide and carbon-monoxide adsorption in zeolitic imidazolate framework materials. J. Phys. Chem. C **114**(5), 2171–2178 (2010). doi:10.1021/jp908058n

Stavitski, E., Pidko, E.A., Couck, S., Remy, T., Hensen, E.J.M., Weckhuysen, B.M., Denayer, J., Gascon, J., Kapteijn, F.: Complexity behind CO_2 capture on NH_2-MIL-53(Al). Langmuir **27**, 3970–3976 (2011)

Su, F., Lu, C., Cnen, W., Bai, H., Hwang, J.F.: Capture of CO_2 from flue gas via multiwalled carbon nanotubes. Sci. Total Environ. **407**(8), 3017–3023 (2009)

Su, F., Lu, C., Kuo, S.-C., Zeng, W.: Adsorption of CO_2 on amine-functionalized Y-type zeolites. Energy Fuels **24**(2), 1441–1448 (2010). doi:10.1021/ef901077k

Torrisi, A., Mellot-Draznieks, C., Bell, R.G.: Impact of ligands on CO(2) adsorption in metal-organic frameworks: first principles study of the interaction of CO(2) with functionalized benzenes. II. Effect of polar and acidic substituents. J. Chem. Phys. **132**(4) (2010). doi:Artn 044705

Tranchemontagne, D.J., Hunt, J.R., Yaghi, O.M.: Room temperature synthesis of metal-organic frameworks: MOF-5, MOF-74, MOF-177, MOF-199, and IRMOF-0. Tetrahedron **64**(36), 8553–8557 (2008). doi:10.1016/j.tet.2008.06.036

Tsuzuki, S., Luthi, H.P.: Interaction energies of van der Waals and hydrogen bonded systems calculated using density functional theory: assessing the PW91 model. J. Chem. Phys. **114**(9), 3949–3957 (2001)

Vaidhyanathan, R., Iremonger, S.S., Dawson, K.W., Shimizu, G.K.H.: An amine-functionalized metal organic framework for preferential CO_2 adsorption at low pressures. Chem. Commun. **35**, 5230–5232 (2009)

Xu, Q., Liu, D., Yang, Q., Zhong, C., Mi, J.: Li-modified metal-organic frameworks for CO_2/CH_4 separation: a route to achieving high adsorption selectivity. J. Mater. Chem. **20**(4) (2010)

Xu, X.C., Song, C.S., Andresen, J.M., Miller, B.G., Scaroni, A.W.: Preparation and characterization of novel CO_2 "molecular basket" adsorbents based on polymer modified mesoporous molecular sieve MCM-41. Microporous Mesoporous Mater. **62**(1–2), 29–45 (2003)

Xue, C., Zhong, C.: Molecular simulation study of hexane diffusion in dynamic metal-organic frameworks. Chin. J. Chem. **27**(3), 472–478 (2009). doi:10.1002/cjoc.200990077

Zhang, L., Wang, Q., Liu, Y.-C.: Design for hydrogen storage materials via observation of adsorption sites by computer tomography. J. Phys. Chem. B **111**(17), 4291–4295 (2007). doi:10.1021/jp0713918

Zheng, C., Liu, D., Yang, Q., Zhong, C., Mi, J.: Computational study on the influences of framework charges on CO_2 uptake in metal–organic frameworks. Ind. Eng. Chem. Res. **48**(23), 10479–10484 (2009). doi:10.1021/ie901000x

Zhou, M., Wang, Q., Zhang, L., Liu, Y.-C., Kang, Y.: Adsorption sites of hydrogen in zeolitic imidazolate frameworks. J. Phys. Chem. B **113**(32), 11049–11053 (2009). doi:10.1021/jp904170s

Zukal, A., Mayerova, J., Cejka, J.: Alkali metal cation doped Al-SBA-15 for carbon dioxide adsorption. Phys. Chem. Chem. Phys. **12**(20) (2010)